I&EC research
Industrial & Engineering Chemistry Research

Article

Cite This: Ind. Eng. Chem. Res. 2018, 57, 6664−6672

pubs.acs.org/IECR

Tuning the Catalytic Activity and Stability of Al−Ti Bimetallic Species Immobilized on $MgO-Al_2O_3-SiO_2$ for 1-Decene Oligomerization

Hui Sun,*[,†] Xingxing Lei,[†] Jialun Tan,[†] Zhongwei Sun,[†] Xiao Han,[†] Jichang Liu,[†] Jigang Zhao,[†] Benxian Shen,[†] Xianghui Zhang,[‡,§] Xiaofeng Guo,[‡,∥] and Di Wu*[,‡,∥,§,⊥]

[†]Petroleum Processing Research Center, East China University of Science and Technology, Shanghai 200237, China

[‡]Alexandra Navrotsky Institute for Experimental Thermodynamics, [§]The Gene and Linda Voiland School of Chemical Engineering and Bioengineering, [∥]Department of Chemistry, and [⊥]Materials Science and Engineering, Washington State University, Pullman, Washington 99163, United States

Supporting Information

ABSTRACT: Immobilization of active components on support materials is an effective strategy to minimize the negative environmental and health impacts of hazardous Lewis acid catalysts. In this study, we synthesized immobilized Al−Ti bimetallic catalysts supported on $MgO-Al_2O_3-SiO_2$ ternary oxide (Al−Ti/MAS) with accurately controlled compositions and pore structures. We also characterized supports and catalysts using various techniques. Further, we examined their catalytic activity and stability using a fixed-bed reactor. Compared with γ-Al_2O_3-derived catalyst, the Al−Ti/MAS catalysts feature more Lewis acid sites and better pore structure accessibility, which lead to much higher activity and stability. Among these MAS samples, M-3 (Si/Al molar ratio = 9.76) presents the highest loading of active species with a chlorine content of 16.7%, leading to the highest PAO yield of 94.6% and the best stability. In addition, the deactivation of the MAS-derived Al−Ti bimetallic catalysts is mainly ascribed to the loss of active species during oligomerization.

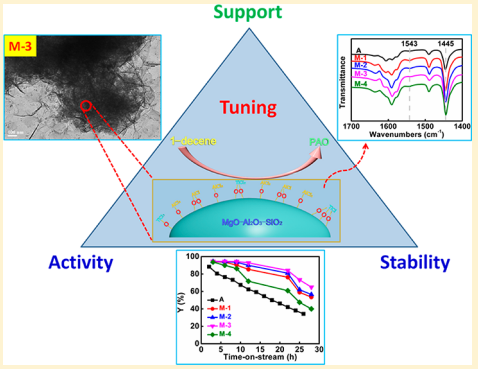

1. INTRODUCTION

Compared with petroleum-derived mineral oils, synthetic poly-α-olefin (PAO) lubricants have great advantages such as excellent thermal and oxidative stability, high viscosity index, great low-temperature fluidity, low volatility, low corrosiveness, and good biodegradability. Therefore, they are extensively applied when mineral oils fail to meet the requirement.[1−5] Typically, PAO lubricants are synthesized through catalytic oligomerization of linear α-olefins (LAO) followed by hydrogenation, in which 1-decene is the most commonly used α-olefin monomers.

The properties of PAO base stocks mainly depend on the degree of polymerization and molecular structures of oligomers, which are tightly correlated to the properties and quality of catalyst used in PAO synthesis.[6] A great variety of catalysts, both homogeneous and heterogeneous, including Lewis acid catalysts,[7] Ziegler − Natta catalysts,[8] metallocene catalysts,[9−11] ionic liquid catalysts,[12] transition metal complexes,[13−16] reduced chromium,[17−19] and other solid acid catalysts,[20−25] have been developed and employed for oligomerization of α-olefins. Considering their highly corrosive and hazardous nature, homogeneous acid catalysts are gradually being replaced by environmentally friendly solid acid catalysts.[26] One effective strategy to minimize the negative environmental impacts of acid catalysts is to immobilize the catalytically active species on porous solid materials.[27−29] Extensive studies on immobilization of aluminum chloride ($AlCl_3$) on solids have been performed. Supports employed include silica, zeolite, and polymer microsphere. These materials were used under laboratory conditions in Mannich-type reaction (silica),[30] isopropylation reaction of naphthalene (zeolite),[31] and Friedel−Crafts acylation reaction of polystyrene (polymer microsphere).[32] However, their limited activity and stability greatly hinder further industrial application of these supported catalysts. In our recent study,[33] a series of supported Al−Ti bimetallic catalysts were synthesized by immobilization of $AlCl_3$ and $TiCl_4$ on several porous materials. The 1-decene oligomerization catalytic tests suggest that γ-Al_2O_3-derived Al−Ti catalyst (Al−Ti/γ-Al_2O_3) is able to deliver high activity yet poor stability. The deactivation of Al−Ti/γ-Al_2O_3 can be ascribed to (i) loss of active species and (ii) pore blockage caused by oligomers which reduces the accessibility of active sites. Thus, further material development is necessary to enhance the activity and stability of Al−Ti bimetallic catalyst supported on oxide materials.

In this work, we applied $MgO-Al_2O_3-SiO_2$ (MAS) ternary oxides as support to immobilize Al−Ti bimetallic catalysts for 1-decene oligomerization. These MAS supports and the catalysts they derived with immobilized Al−Ti active species

Received: February 17, 2018
Revised: April 26, 2018
Accepted: April 30, 2018
Published: April 30, 2018

DOI: 10.1021/acs.iecr.8b00791
Ind. Eng. Chem. Res. 2018, 57, 6664−6672

were characterized thoroughly. We further tested their catalytic performance by performing oligomerization of 1-decene using a fixed-bed reactor, in which we observed enhanced catalyst activity and stability compared with oligomerization using Al−Ti/γ-Al_2O_3. By accurate manipulation of compositional and structural factors of MAS, we are able to adjust the surface Lewis acidity and pore structure for oligomerization of α-olefins and to correlate the structure−activity−stability relationships. Such fundamental insight is critical toward understanding of synthesis, application, and deactivation of these ternary oxide supported catalysts for oligomerization.

2. EXPERIMENTAL METHODS

2.1. Materials and Reagents. The reagents used include 1-decene (purity >95%, Shanghai Yangyang Industrial Co., Ltd., China), anhydrous aluminum trichloride, and hydrated magnesium nitrate from Sinopharm Chemical Reagent Co., Ltd., China (purity >98%), carbon tetrachloride (purity >98%, Shanghai Titan Scientific Co., Ltd., China), and titanium tetrachloride, hydrated aluminum nitrate, and nitric acid from Shanghai LingFeng Chemical Reagent Co., Ltd., China (purity >98%). Silica sol (Qingdao Mike Silica Gel Desiccant Co., Ltd., China) has a SiO_2 content of 30%, and its colloidal particle diameter ranges from 10 to 20 nm. γ-Al_2O_3 (Sinopharm Chemical Reagent Co., Ltd., China) is used as a reference support.

2.2. Preparation of MAS Supports. A series of MAS supports were prepared by a coprecipitation method. First, 39.6 g of $Al(NO_3)_3{\cdot}9H_2O$ and 28.2 g of $Mg(NO_3)_2{\cdot}6H_2O$ were dissolved in an acid solution containing 6 g of HNO_3 and 52.8 g of deionized water. The resultant solution was gradually dripped into silica sol under stirring at room temperature to obtain a slurry mixture. Then, the mixture was heated at 50 °C for 24 h followed by dehydration at 130 °C in an oven to form the MgO−Al_2O_3−SiO_2 (MAS). The chemical composition of the MAS can be further tuned by variation of the Al/Si ratio. Eventually, the MAS samples were triturated with a mortar and sieved to obtain samples with different particle sizes. All MAS ternary oxide samples were thermally treated using the following procedure: (i) heating the sample from room temperature to 300 °C at 3 °C/min and holding at 300 °C for 3 h and (ii) further increasing temperature to 600 °C at 3 °C/min and retaining for 3 h.

2.3. Preparation of Immobilized Al−Ti Bimetallic Catalysts and Oligomerization. The catalyst preparation was achieved by loading the active species, $AlCl_3$ and $TiCl_4$, onto various support materials, including γ-Al_2O_3 (reference support) and four MAS with different chemical compositions. Carbon tetrachloride was used as solvent in all the immobilization experiments. The detailed immobilization procedure has been described elsewhere.[33] The samples were labeled as A, M-1, M-2, M-3, and M-4 (see Table S1) for catalysts supported by γ-Al_2O_3 and MAS-1, -2, -3, and -4, respectively. We used as-made catalyst sample from the same batch for characterization and catalytic oligomerization of 1-decene in a fixed-bed reactor (see Figure 1) according to the procedure described in our previous publication. In this study, the liquid hourly space velocity (LHSV) for oligomerization of 1-decene was set to be at 1 h^{-1}.

The yield of PAO product, Y, can be calculated using the equation

$$Y = m_P/m_D \times 100\%$$

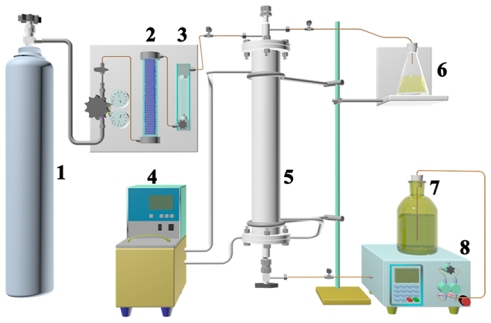

1 - N_2 cylinder, 2 - dryer, 3 - flowmeter, 4 - temperature controller, 5 - fixed-bed reactor, 6 - product tank, 7 - raw material tank, 8 - pump.

Figure 1. Flowchart for oligomerization.

in which m_P and m_D represent the mass of the >280 °C fraction in the oligomerization product and the mass of reactant 1-decene, respectively. Y_0 is the yield corresponding to the initial products obtained within the first 3 h TOS.

2.4. Sample Characterizations. The compositions of oligomers were analyzed using a GC-14C gas chromatograph (Shimadzu Co., Japan) equipped with a flame ionization detector. Kinematic viscosities of the synthetic PAO products were measured using a SYD-265C viscosity meter (Shanghai Geological Instrument Factory, China) according to ASTM D445. The kinematic viscosity of PAO products was tested at 40 and 100 °C, denoted as ν_{40} and ν_{100}, respectively. The viscosity index (VI) was derived from ν_{40} and ν_{100} according to ASTM D2270, and the freezing point (FP) was measured on a SYP1022-2 freezing point analyzer (Shanghai Boli Instrument Co., Ltd., China). The chlorine contents in the synthetic PAO products were determined using a WK-2D microcoulometric analyzer (Jiangfen Electroanalytical Instrument Co., Ltd., China).

The chlorine contents of all catalysts were determined using a ZWC-2001 salt content analyzer (Jiangsu Jierui Instrument and Equipment Co., Ltd., China). One gram of catalyst was immersed in 100 mL of 0.5 mol/L nitric acid solution for 12 h and washed at least for three times with deionized water. For each catalyst, the treating solution was collected and diluted to 1000 mL with deionized water. The mass fraction of chlorine in each catalyst, X_{Cl}, was simply calculated by the equation $X_{Cl} = 1000C_0/M_0$, in which C_0 is the chlorine content in treating nitric acid solution (g mL^{-1}). M_0 is the mass of fresh or deactivated catalyst sample (g).

The chemical compositions of supports and catalysts were determined via element map scanning carried out at a Falcon energy-dispersive spectrometer (EDS) (EDAX Inc., USA). Five to eight points were measured at different positions to obtain an average elemental composition.

The specific surface area and pore diameter distribution of supports and immobilized catalysts were characterized by a 3H-2000SP4 microstructure analyzer (Best Technology Co., Ltd., China). All samples were degassed at 300 °C for 5 h under vacuum and tested in the pressure range of 0.4−101.8 kPa. Thermogravimetry (TGA) analyses were conducted on a SDT Q600 system (TA Instruments, USA). Sample pellets were placed in a platinum crucible and heated from room temperature to 800 °C at 10 °C/min under the oxygen flow (100 mL/min).

DOI: 10.1021/acs.iecr.8b00791
Ind. Eng. Chem. Res. 2018, 57, 6664−6672

XPS spectra of all samples were obtained using a Thermo Scientific ESCALAB 250Xi spectrometer (Thermo Fisher Scientific, USA) equipped with a Mg anode (14 kV, 250 W). Adsorbed pyridine infrared (Py-IR) analyses were performed on a V70 Fourier transform infrared spectroscopy (Bruker, Germany). The powder samples were pressed into a 13 mm translucent pellets, degassed in vacuum at 300 °C for 2 h, and then cooled down to 100 °C under dynamic vacuum. Pyridine adsorption experiments were conducted, and then the pyridine-equilibrated samples were desorbed successively at 150 and 400 °C through a temperature-programmed route.

Morphologies of support and catalyst samples were determined by using a transmission electron microscope (TEM) (JEM-2100, JEOL). Samples were made by ultrasonication in ethanol for 15 min followed by dropping the suspension onto carbon coated 400 mesh copper grids. Images were collected using a slow scanning CCD camera.

3. RESULTS AND DISCUSSION

3.1. Support−Activity Relations. Support material plays a crucial role in determination of the active species immobilization and the catalytic performance of catalyst by providing specific binding sites and pore structures.[34] Both alumina (Al_2O_3) and silica (SiO_2) exhibit strong binding affinity for the Al−Ti active species.[35,36] Such binding affinity is critical to enable effective support for heterogeneous Lewis acid catalytically active species for olefin polymerization.[37] Similarly, magnesium oxide (MgO) is also a good support material for immobilization of Lewis acid catalysts.[38,39] MgO surface is hydroxyl-rich, which can coordinate aluminum chloride and titanium tetrachloride forming a variety of active sites.[40,41] The interactions between Mg and active species are considered to greatly enhance (active species) loading and catalytic activity.[42] In our study, we prepared the $MgO−Al_2O_3−SiO_2$ ternary oxide materials via coprecipitation and employed them as supports for the impregnated Al−Ti bimetallic active components. The chemical compositions of all samples synthesized are listed in Table S2 (on Al_2O_3 basis). Specifically, the Si/Al molar ratio increases from 4.86 for sample M-1 to 12.30 for M-4, while the Mg/Al molar ratio ranges from 0.904 for M-2 to 1.061 for M-3. The measured molar ratios for both Si/Al and Mg/Al are in good agreement with the corresponding stoichiometry of the initial reactant mixtures. Interestingly, significant impact of chemical composition on the pore structure of support was observed (see Table 1). We also include the data for γ-Al_2O_3 support used in our earlier study as reference. Compared with γ-Al_2O_3 support, all MAS supports present smaller specific surface area (S_{BET}) and larger average pore size (d_p) (see Figure 2). In addition, as Si/Al molar ratio increases, the MAS supports exhibit monotonically decreasing specific surface area and increasing average pore dimension.

Table 1. BET Specific Surface Area, Pore Volume, and Average Pore Diameter of Various Supports

support	S_{BET} [a] (m^2/g)	V_p [b] (cm^3/g)	d_p [c] (nm)
A	281.38	0.44	6.25
M-1	192.38	0.36	7.40
M-2	167.59	0.40	9.46
M-3	154.47	0.40	10.41
M-4	148.62	0.40	10.81

[a]Specific surface area. [b]Pore volume. [c]Average pore diameter (1.7−300 nm).

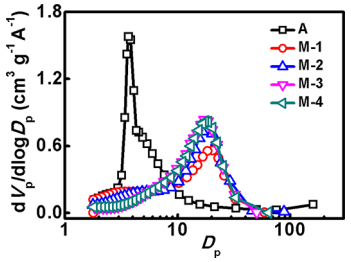

Figure 2. Pore size distribution for different supports.

Well-defined chemical composition and narrow pore size distribution are two critical factors governing the surface homogeneity of Al−Ti/MAS, and catalytic selectivity of 1-decene oligomerization. Chemical composition analyses (see Table S2) coupled with chlorine content measurements (see Figure 3) suggest immobilization of $AlCl_3$ and $TiCl_4$. All Al−Ti/MAS catalysts have higher chlorine contents than that of Al−Ti/γ-Al_2O_3 sample. Our present findings and previous results[33] confirm that there is no strong dependence of active specie loading on the specific surface area of catalyst. More specifically, the chlorine contents of catalysts rank in the following sequence: M-3 > M-2 > M-1 (M-4) > A. Meanwhile, the PAO yields present the same order, with M-3 showing the highest yield. Such linear dependence of Y_0 on X_{Cl} with a positive slope is in excellent agreement with what we observed in an earlier study. Among these MAS samples, M-3 (Si/Al molar ratio = 9.76) presents the highest loading of active species with a chlorine content of 16.7% leading to the highest PAO yield of 94.6%.

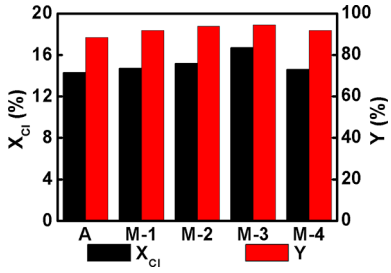

Figure 3. Chlorine content (X_{Cl}) and PAO yield (Y) of catalysts with different supports.

In addition, XPS analyses reveal the distribution of Al and Ti species on support surfaces (Figure 4). Similar to catalyst A (using γ-Al_2O_3 as support), all four MAS supported samples, M-1, M-2, M-3, and M-4, show Al $2p_{1/2}$, Ti $2p_{1/2}$ and Ti $2p_{3/2}$ doublet, corresponding to the oxygenated states of Al and Ti, respectively. The binding energy of Ti $2p_{3/2}$ increases from 458.7 to 459.0 eV for A and M1 to 459.5−459.9 eV for M2, M3, and M4. The Ti species are found to exist in two forms,[43,44] Ti−O−Al for A and M1 catalysts and Ti−O−Si for M2, M3, and M4 samples, indicating distinctly different binding states for Ti species loaded on MAS supports as Si/Al molar ratio varies. Our previous[27] Al MAS NMR studies on γ-Al_2O_3 or SiO_2-derived catalyst suggest that the $AlCl_3$ species may be coordinated by the surface oxygen of supports. According to the XPS analysis and chloride content measurement, the

DOI: 10.1021/acs.iecr.8b00791
Ind. Eng. Chem. Res. 2018, 57, 6664−6672

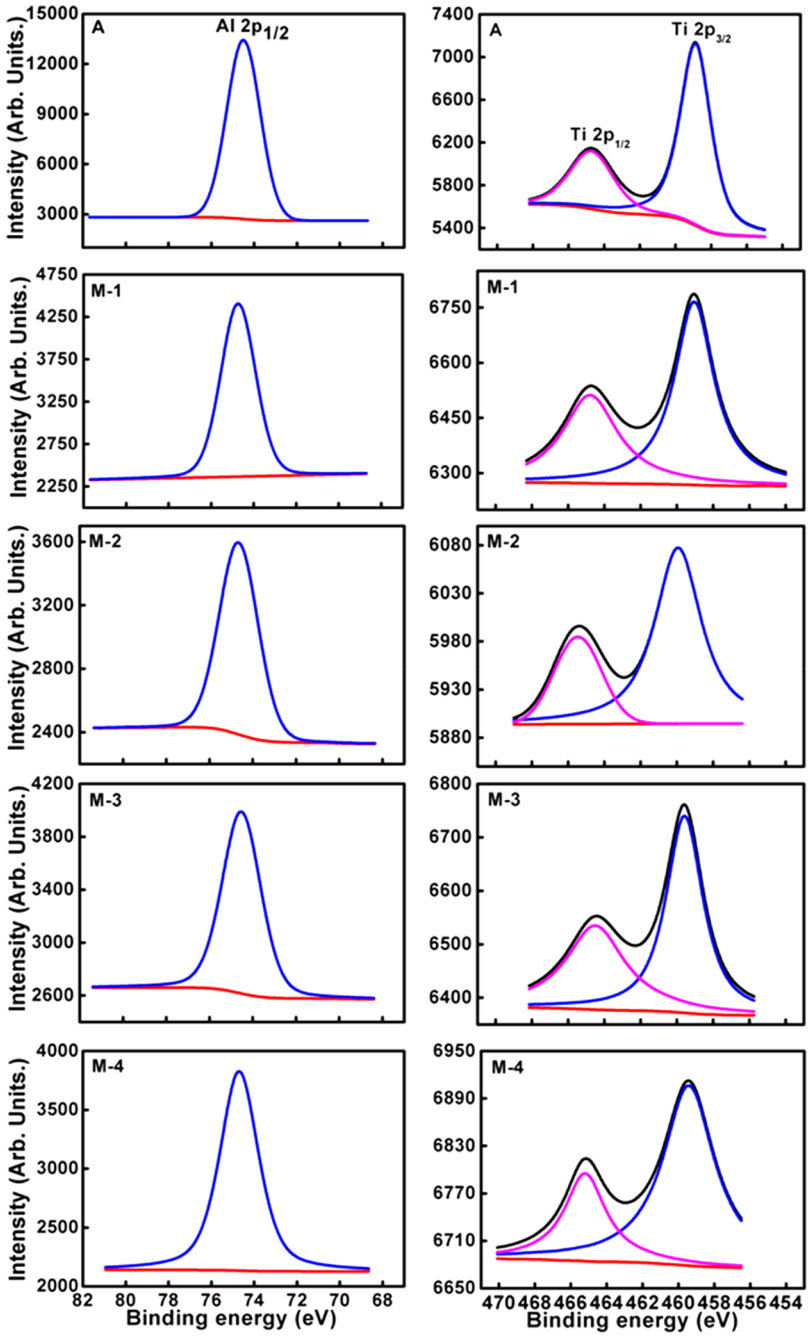

Figure 4. Al/Ti XPS spectra for different catalysts.

relative Al/Ti ratios for the bimetallic active species immobilized on different supports can be estimated (see Figure 5a). Specifically, the Al/Ti ratio is up to 12 for M-3, and is as low as 2.5 for A. These values are very close to those obtained from EDS analyses. However, they drivative from the initial Al/Ti molar ratio (Al/Ti = 5) we used during the $AlCl_3$ and $TiCl_4$ immobilization process. The Al/Ti molar ratios mimic the trends of chlorine contents and PAO yields for samples with different support materials. We conclude that the catalytic activity is determined by the loading of Al species. The weak affinity of γ-Al_2O_3 for Al species results in low Al immobilization, which leads to a low PAO yield (88.4% for the first 3 h TOS).

We also characterized the acidity of all catalysts by Py-IR (see Figure 5b). All samples show a strong absorption peak at about 1445 cm^{-1}, corresponding to pyridine adsorption on Lewis acid sites.[45,46] Compared with γ-Al_2O_3-derived catalyst (A), all MAS supported catalysts (M-1, M-2, M-3, and M-4) feature more Lewis acid sites exhibiting one much more significant absorption event at 1445 cm^{-1}. Additionally, a weak signal at 1543 cm^{-1} assigned to pyridinium ions adsorbed at Brønsted acid sites[45] is observed for all MAS supported catalysts. Interestingly, this peak can be hardly seen for catalyst A. All these results point out that higher Lewis acid site concentration leads to the enhanced catalytic activity. Moreover, all samples present a peak with moderate intensity at 1490 cm^{-1}, which can be attributed to coexistence and coupling of Brønsted and Lewis acid sites.[47]

To further elucidate the binding of active species on each support, TG analyses were conducted in oxygen atmosphere

DOI: 10.1021/acs.iecr.8b00791
Ind. Eng. Chem. Res. 2018, 57, 6664−6672

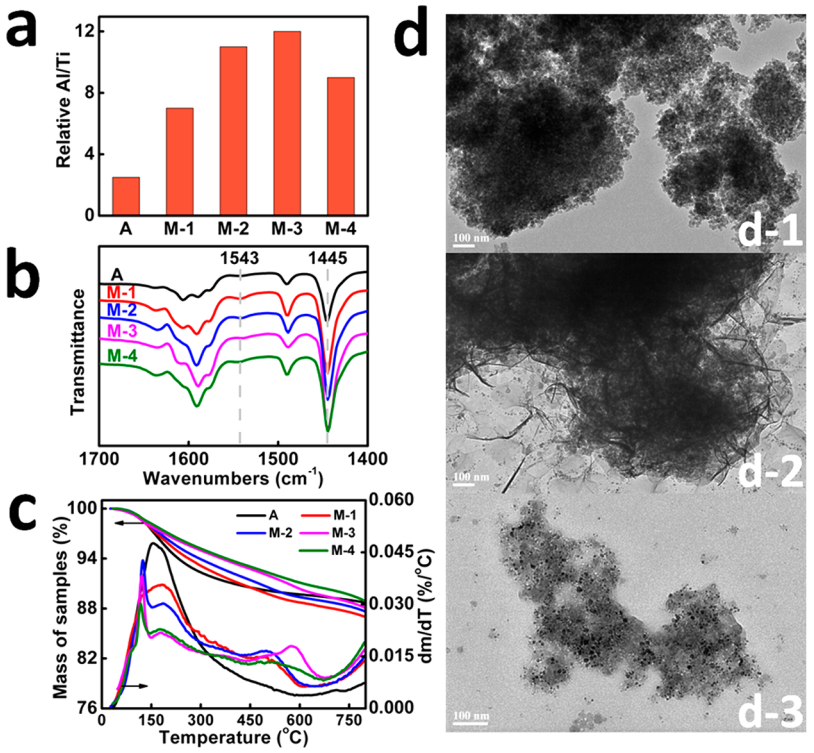

Figure 5. (a) Relative Al/Ti molar ratios on sample surfaces. (b) Py-IR spectra. (c) TG-DTG curves for A, M-1, M-2, M-3, and M-4 catalysts. (d) TEM images for M-3 support (d-1), fresh (d-2), and used (d-3) M-3 catalysts.

(see Figure 5c). Sample A shows a continuous weight decrease upon heating from room temperature (RT) with merely one broad peak spanning from 150 to 200 °C on the DTG curve. In contrast, the DTG curves of all MAS supported catalysts feature two weight loss regions: the low temperature weight loss events (region I), spanning from RT to 300 °C, and the high temperature events (region II), ranging from 420 to 670 °C. Specifically, in region I, the DTG peak of M-1 is very similar as that of A. Nevertheless, all other MAS supported catalysts with Si/Al > 6.6 present two peaks. Specifically, a sharp peak (peak I) was observed at 124, 122, and 119 °C for M-2, M-3, and M-4, respectively, while a much broader peak (peak II) centered at 186, 179, and 174 °C was found for M-2, M-3, and M-4, respectively. Considering the low sublimation temperature of $AlCl_3$ and low boiling point of $TiCl_4$, both below 200 °C, we conclude that the low temperature weight loss corresponds to the release of free active species from the catalysts under thermal treatment. Furthermore, since all MAS supports were subjected to thermal treatment at temperature up to 600 °C prior to immobilization experiments, the weight loss is attributed to the desorption of immobilized active species. In other words, this group of active species interact with the strong binding sites of supports supported by higher desorption temperature observed in region II. Interestingly, broad DTG peaks were observed in region II spanning from 500 to 580 °C, an indication of active species−support binding on a spectrum of sites with different energetic states. In comparison with support A, all MAS supports feature stronger binding sites resulting from the specific chemical composition of ternary oxide. Specifically, Mg species can coordinate Al−Ti active species to enhance the immobilization.

To gain further insights into the immobilization and migration of active species on the MAS supports, TEM images were taken for the M-3 support, fresh, and deactivated M-3 derived catalysts (see Figure 5d). The M-3 support is found to be well-dispersed nanoparticles with relatively uniform particle size (10−20 nm). The M-3 supported catalyst shows a spongelike morphology, indicating well-distributed active species on the nanoparticle supports. Accordingly, when the spent M-3 supported catalyst undergone 28 h of time-on-stream (TOS), the spongelike active species disappeared due to active specie loss. Instead, MAS particle aggregation and growth was observed.

3.2. Support−Stability Relations. The catalytic stability of all catalysts was evaluated using a continuously operated fixed-bed reactor. The PAO yield is plotted as a function of TOS in Figure 6a. Despite similar initial PAO yields (Figure 3), all samples show decreasing yields with different slopes as TOS increases, suggesting catalytic deactivation at various rates. Specifically, the PAO yield decreases to 73.3% at 25 h for M-3, 47.5% at 25 h for M-4, and 38.1% at 24 h for A. Generally, catalysts supported by MAS materials demonstrate better stability compared with catalyst supported by γ-Al_2O_3. Such differences in stability were determined by the strength of binding between (i) support material and immobilized active components and (ii) the structural evolution of catalysts during 1-decene oligomerization. On one hand, impregnation of $AlCl_3$ leads to reactions between $AlCl_3$ and the surface hydroxyls of support materials accompanied by HCl release.[20,48,49] $AlCl_3$ exists on the support surface in the form of $(-M-O)_x-AlCl_y$. In our case, M represents Al, Si, or Mg, with $x + y = 3$. When $x = 0$, $(-M-O)_0-AlCl_3$ represents free $AlCl_3$.[20,50,51] Similarly, immobilized $TiCl_4$ also exhibits in bonded and free $TiCl_4$ forms.[52,53] Typically, strongly bonded $(-M-O)_1-AlCl_2$ ($x = 1$) species are considered to be the main contributor providing the catalytic activity.[51,54] In contrast, the free $AlCl_3$ active species merely have weak interactions with the support without defined bonding. Consequently, as reaction proceeds, the

DOI: 10.1021/acs.iecr.8b00791
Ind. Eng. Chem. Res. 2018, 57, 6664−6672

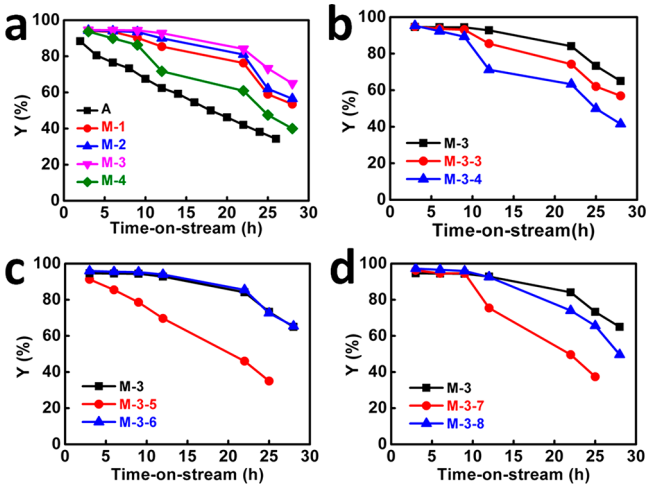

Figure 6. PAO yield (Y) of catalysts prepared with (a) different supports (LHSV is 1 h^{-1} for catalysts M-1, M-2, M-3, and M-4 and 0.5 h^{-1} for catalyst A[33]), (b) M-3 supports with a series of particle sizes, (c) different starting $AlCl_3$ dosages, and (d) different starting Al/Ti ratios for immobilization.

continuous loss of free $AlCl_3$ species leads to significant decrease in catalytic activity. According to our characterizations, MAS supports feature stronger affinity to surface adsorbed Al and Ti species compared with γ-Al_2O_3 support. On the other hand, the MAS-derived catalysts have larger pore size resulting in less pore blockage caused by oligomers and less surface site deactivation compared with γ-Al_2O_3 supported catalyst. The enhanced stability observed for the MAS-derived catalysts is owing to both surface and structural factors, including the hydroxyl group concentration and pore structure accessibility.

3.3. Support Particle Size Effects. To evaluate the impact of particle size on the activity and stability of all catalysts, three MAS samples with particle sizes of 10−20 mesh (M-3), 20−40 mesh (M-3-3), and 40−60 mesh (M-3-4) were prepared and tested for immobilization of Al−Ti active species (see Figure 6b). As the particle size of support decreases, the corresponding catalysts exhibit slightly increasing chlorine contents and initial yields. M-3, M-3-3, and M-3-4 show (X_{Cl}, Y_0) of (16.7%, 94.6%), (16.8%, 94.9%), and (18.3%, 95.3%), respectively. However, interestingly, their stability decrease exhibits distinctly different trends. Specifically, the M-3 sample with the largest particle size demonstrates the highest stability with a yield, Y, of 92.8% at 12 h and 65.0% at 28 h. The sample with the smallest particle size, M-3-4, shows the steepest decaying activity trend with a Y of 71.2% at 12 h and 41.5% at 28 h. The loss of active species has been confirmed to be one of the most critical reasons for deactivation of immobilized catalysts.[33] In this study, it is very likely that the significant impact of particle size on catalyst stability is governed by the rate of active species loss from the support materials, in which particles with smaller sizes (higher surface areas) may lead to faster loss of active species during the oligomerization process.

3.4. Impact of Immobilization Temperature. The catalytic performances for catalysts prepared at different immobilization temperatures are presented in Table 2. As the immobilization temperature increases from 60 to 80 °C, X_{Cl} increases from 13.1 to 16.7%, while the initial product yield Y_0 remains constant. This suggests substantial active specie loading on the supports at all temperatures. Considering the low boiling point of solvent, CCl_4 (76.8 °C) we used, all immobilization

Table 2. Effect of Immobilization Temperature on Chlorine Content of Supported Catalyst and Oligomerization

catalyst	T_i (°C)	X_{Cl} (%)	Y_0[a] (%)	ν_{40} (mm^2/s)	ν_{100} (mm^2/s)	VI	FP (°C)
M-3-1	60	13.1	93.8	72.5	11.3	148	−72
M-3-2	70	13.7	93.9	77.0	12.1	154	−71
M-3	80	16.7	94.6	85.1	13.2	156	−68

[a]Initial PAO yield.

experiments are carried out at temperatures below 80 °C. Indeed, immobilization is a complicated process, which is governed by integrated effects of temperature, treatment length (time), and the property of the solvent.[55] The immobilization temperature determines the diffusion rate of active species in liquid solvent and on support material surfaces once the solvent and time of immobilization are defined. Higher immobilization temperature can boost the reflux of CCl_4 solvent, accelerating the diffusion of active species into porous structures of supports, which directly leads to higher chlorine loading for better catalytic performance of 1-decene oligomerization. In our study, the PAO product synthesized using M-3 catalyst with the highest chlorine content of 16.7% shows higher kinetic viscosities (85.1 mm^2/s for ν_{40} and 13.2 mm^2/s for ν_{100}), viscosity index, and freezing point (−68 °C), suggesting a higher degree of oligomerization and lower branch ratio—the ratio of methyl to methylene groups in the oligomer. M-3-1 having chlorine content of 13.1% exhibits lower kinetic viscosities, viscosity index, and freezing point.

3.5. Role of Active Component Loading. The impact of active component loading on immobilization and oligomerization was examined at a fixed Al/Ti ratio as $AlCl_3$/support mass ratio varies. Our results suggest that the sample chlorine content has a strong dependence on the $AlCl_3$/support mass ratio, $m(AlCl_3)/m(support)$. Specifically, the chlorine content increases from 10.7% for M-3-5 to 19.5% for M-3-6 as $m(AlCl_3)/m(support)$ increases from 0.35 to 0.45 (see Table 3). Accordingly, Y_0 increases from 91.3% (M-3-5) to 95.9% (M-3-6). Higher loading enables more active sites promoting PAO chain growth and leading to increased kinetic viscosities for the PAO products. Further, we also plotted the PAO yields at different TOS in Figure 6c. Among all three catalyst samples, M-3 and M-3-6 have nearly the same activity and deactivation trend, while M-3-5, the sample with the least active component loading, shows the quickest deactivation with PAO yield of 46% at 22 h. In contrast, 85.5% yield was achieved for M-3-6 at the same TOS. Therefore, we conclude that the loss of active species is one of the most critical factors leading to deactivation of the catalysts studied. Because of its lower loading of active species, M-3-5 shows much quicker activity decay than M-3 and M-3-6 as TOS increases.

3.6. Al/Ti Molar Ratio: The Synergistic Catalyst and Cocatalyst. The impact of starting Al/Ti molar ratio on impregnation of active species and catalytic oligomerization of 1-decene was evaluated. We fixed the total dosage of $AlCl_3$ and $TiCl_4$ as constant and vary the Al/Ti molar ratio (see Figure 6d and Table 4). We found that all three catalysts exhibit similar initial PAO yield, Y_0; however, they show distinct deactivation rate as reaction proceeds. Interestingly, as Al/Ti molar ratio varies, both X_{Cl} and Y_0 increase followed by a decreasing trend. Additionally, the properties of PAO products show consistent trend for all products. It is found that M-3 (Al/Ti = 5) has the highest stability exhibiting the lowest rate of deactivation. The

DOI: 10.1021/acs.iecr.8b00791
Ind. Eng. Chem. Res. 2018, 57, 6664−6672

Table 3. Effect of $AlCl_3$ Dosage on Chlorine Content of Supported Catalyst and Oligomerization

catalyst	$m(AlCl_3)/m$(support)	X_{Cl} (%)	Y_0 (%)	v_{40} (mm^2/s)	v_{100} (mm^2/s)	VI	FP (°C)
M-3-5	0.35	10.7	91.3	79.1	12.3	153	−69
M-3	0.4	16.7	94.6	85.1	13.2	156	−68
M-3-6	0.45	19.5	95.9	90.6	13.5	151	−67

Table 4. Effect of Al/Ti Molar Ratio on Chlorine Content of Supported Catalyst and Oligomerization

catalyst	n(Al)/n(Ti)	X_{Cl} (%)	Y_0 (%)	v_{40} (mm^2/s)	v_{100} (mm^2/s)	VI	FP (°C)
M-3-7	3	20.7	96.3	91.1	13.7	153	−66
M-3	5	16.7	94.6	85.1	13.2	156	−68
M-3-8	7	22.0	97.2	96.4	14.5	156	−65

great catalytic activity observed here for the Al−Ti bimetallic catalysts is owing to the coupling effects between the catalyst (Al contents) and cocatalyst (Ti species). Compared with M-3-5, the M-3-7 sample with higher Ti loading shows higher PAO yield (75.4%) at 12 h of TOS. This indicates that Ti species play critical role triggering the oligomerization. Previous studies suggest that when the ratio of catalyst to cocatalyst is optimized, bimetallic catalyst achieve the best catalytic activity.[56,57] Such conclusion is in excellent agreement with our study.

3.7. Deactivation Mechanism for MAS Supported Al−Ti Bimetallic Catalysts. As we previously described, all MAS-derived Al−Ti bimetallic catalysts undergo activity loss during catalytic oligomerization of 1-decene. To reveal the underlying deactivation mechanism, we started with the determination of chlorine contents of fresh and spent M-3 catalysts. It is found that the chlorine contents of fresh and used catalysts are 16.7% and 8.1%, respectively, indicating the loss of active species from the support. Additionally, the chlorine contents in PAO products collected at different TOS were also measured. The results for catalysts M-3 and A are presented in Figure 7. The

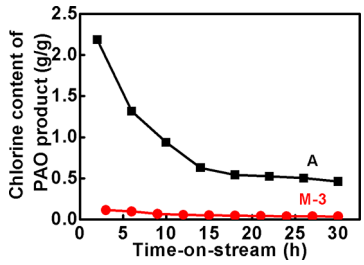

Figure 7. Chlorine contents for PAO products using A and M-3 catalysts.

transfer of active species from support to PAO products can be clearly observed for both catalysts. Specifically, PAO products synthesized using M-3 as catalyst has much lower chlorine content than what the PAO produced using catalyst A. Such phenomenon suggests that, compared with A, M-3 lost less active species. The results strongly support our previous conclusion that MAS support has stronger affinity to the active species compared with that of γ-Al_2O_3. On the other hand, the surface area and pore structure of catalysts are considered to be another two crucial factors for catalyst deactivation in oligomerization. The surface area and pore size analyses of fresh and used M-3 catalyst are listed in Table 5. Upon active species loading the specific surface area and pore volume

Table 5. BET Specific Surface Area, Pore Volume, and Average Pore Diameter of Fresh and Used M-3 Catalysts

sample	S_{BET} (m^2 g^{-1})	V_p (cm^3 g^{-1})	d_p (nm)
fresh M-3	91.82	0.25	11.00
used M-3	102.35	0.24	10.03

decreases, whereas the average pore size increases (see Table 1). This indicates that the active species introduced tends to fill smaller pores first. In contrast, after catalytic deactivation, the M-3 catalyst shows increased specific surface area, from 91.82 to 102.35 m^2/g, and decreased average pore size from 11.00 to 10.03 nm. Clearly, this is due to the loss of micropore-confined active species on M-3 catalyst, resulting in increase of accessible surface and decrease of average pore size. Therefore, we conclude that the deactivation of the MAS-derived Al−Ti bimetallic catalysts is mainly ascribed to the loss of active species during oligomerization. Compared with γ-Al_2O_3-derived catalyst, the catalysts prepared by using MAS as supports exhibit smaller changes in pore structure and, thus, feature much higher activity and stability.

4. CONCLUSIONS

A series of MgO−Al_2O_3−SiO_2 (MAS) were synthesized and employed as catalytic supports for Al−Ti active species. Oligomerization of 1-decene on these MAS-supported Al−Ti catalysts was studied using a fixed-bed reactor. As Si/Al molar ratio increases, the MAS support presents decreasing specific surface area and increasing average pore size. These supports with well-defined compositions enable controllable pore structure and predictable tunability in both catalyst immobilization and catalysis. The M-3 catalysts (Si/Al = 9.76) present higher loading of active species with better catalytic activity and stability. Such enhancement is owing to increased surface hydroxyl concentration and pore accessibility, leading to stronger affinity to active species (more catalytic compounds) and less hindrance to oligomers (less pore blockage). Finally, the loss of active species is concluded to be the most critical factor resulting in deactivation of MAS-derived Al−Ti bimetallic catalysts.

■ ASSOCIATED CONTENT

Supporting Information

The Supporting Information is available free of charge on the ACS Publications website at DOI: 10.1021/acs.iecr.8b00791.

Table of detailed parameters for preparation of supported catalysts and table of chemical compositions for different supports and catalysts (PDF)

■ AUTHOR INFORMATION

Corresponding Authors

*E-mail: sunhui@ecust.edu (H.S.).
*E-mail: d.wu@wsu.edu (D.W.).

ORCID

Hui Sun: 0000-0002-8544-756X

DOI: 10.1021/acs.iecr.8b00791
Ind. Eng. Chem. Res. 2018, 57, 6664−6672

Jichang Liu: 0000-0002-5295-1778
Jigang Zhao: 0000-0002-2773-7200
Di Wu: 0000-0001-6879-321X

Notes

The authors declare no competing financial interest.

■ ACKNOWLEDGMENTS

This work is financially supported by the Training Program of the Major Research Plan of the National Natural Science Foundation of China (Grant 91634112), the Natural Science Foundation of Shanghai (Grant 16ZR1408100), and the Open Project of State Key Laboratory of Chemical Engineering (SKL-ChE-16C01). D.W. acknowledges institutional funds from the Gene and Linda Voiland School of Chemical Engineering and Bioengineering at Washington State University. X.Z. was supported by the Chambroad Distinguished Fellowship.

■ REFERENCES

(1) Brennan, J. A. Wide-temperature range synthetic hydrocarbons fluids. *Ind. Eng. Chem. Prod. Res. Dev.* **1980**, *19* (1), 2−6.
(2) Lappin, G. R.; Sauer, J. D. *Alpha Olefin Application Handbook*; Marcel Dekker: New York, 1989.
(3) Rudnick, L. R.; Shubkin, R. L. *Synthetic Lubricants and High-Performance Functional Fluids*, revised and expanded; CRC Press: 1999.
(4) Murphy, W. R.; Blain, D. A.; Galiano-Roth, A. S.; Galvin, P. A. Benefits of synthetic lubricants in industrial applications. *J. Synth. Lubr.* **2002**, *18* (4), 301−325.
(5) Boyde, S. Environmental benefits and impacts of lubrication. *Green Chem.* **2002**, *4* (4), 293−307.
(6) Park, J. H.; Jang, Y. E.; Jeon, J. Y.; Go, M. J.; Lee, J.; Kim, S. K.; Lee, S.-I.; Lee, B. Y. Preparation of ansa-metallocenes for production of poly(α-olefin) lubricants. *Dalt. Trans.* **2014**, *43* (26), 10132−10138.
(7) Constant, S.; Basset, C.; Dumas, C.; Di Renzo, F.; Robitzer, M.; Barakat, A.; Quignard, F. Reactive organosolv lignin extraction from wheat straw: influence of lewis acid catalysts on structural and chemical properties of lignins. *Ind. Crops Prod.* **2015**, *65*, 180−189.
(8) Sinn, H.; Kaminsky, W.; VOLLMER, H.; Woldt, R. Living polymers' with Ziegler catalysts of high productivity. *Angew. Chem.* **1980**, *92*, 396−402.
(9) Alt, H. G.; Köppl, A. Effect of the nature of metallocene complexes of group IV metals on their performance in catalytic ethylene and propylene polymerization. *Chem. Rev.* **2000**, *100* (4), 1205−1221.
(10) Coates, G. W. Precise control of polyolefin stereochemistry using single-site metal catalysts. *Chem. Rev.* **2000**, *100* (4), 1223−1252.
(11) Gromada, J.; Carpentier, J. F.; Mortreux, A. Group 3 metal catalysts for ethylene and alpha-olefin polymerization. *Coord. Chem. Rev.* **2004**, *248* (3−4), 397−410.
(12) He, Y.; Zhang, Q.; Zhan, X.; Cheng, D.; Chen, F. Synthesis of efficient SBA-15 immobilized ionic liquid catalyst and its performance for Friedel−Crafts reaction. *Catal. Today* **2016**, *276*, 112−120.
(13) Gibson, V. C.; Spitzmesser, S. K. Advances in non-metallocene olefin polymerization catalysis. *Chem. Rev.* **2003**, *103* (1), 283−315.
(14) Kermagoret, A.; Braunstein, P. SHOP-type nickel complexes with alkyl substituents on phosphorus, synthesis and catalytic ethylene oligomerization. *Dalt. Trans.* **2008**, *33* (6), 822−831.
(15) Bianchini, C.; Giambastiani, G.; Luconi, L.; Meli, A. Olefin oligomerization, homopolymerization and copolymerization by late transition metals supported by (imino)pyridine ligands. *Coord. Chem. Rev.* **2010**, *254* (5−6), 431−455.
(16) McGuinness, D. S. Olefin oligomerization via metallacycles: dimerization, trimerization, tetramerization, and beyond. *Chem. Rev.* **2011**, *111* (3), 2321−2341.
(17) Theopold, K. H. Homogeneous chromium catalysts for olefin polymerization. *Eur. J. Inorg. Chem.* **1998**, *1998*, 15−24.
(18) Zhang, H.; Huang, J. L.; Qian, Y. L. Progress in synthesis of homogeneous chromium catalysts and their application in olefin polymerization. *Chinese J. Org. Chem.* **2002**, *22* (12), 981−989.
(19) Wasserscheid, P.; Grimm, S.; Köhn, R. D.; Haufe, M. Synthesis of synthetic lubricants by trimerization of 1-decene and 1-dodecene with homogeneous chromium catalysts. *Adv. Synth. Catal.* **2001**, *343* (8), 814−818.
(20) Drago, R. S.; Getty, E. E. Preparation and catalytic activity of a new solid acid catalyst. *J. Am. Chem. Soc.* **1988**, *110* (10), 3311−3312.
(21) Chen, C. S. H.; Bridger, R. F. Shape-selective oligomerization of alkenes to near-linear hydrocarbons by zeolite catalysis. *J. Catal.* **1996**, *161* (230), 687−693.
(22) Van Grieken, R.; Escola, J. M.; Moreno, J.; Rodríguez, R. Liquid phase oligomerization of 1-hexene over different mesoporous aluminosilicates (Al-MTS, Al-MCM-41 and Al-SBA-15) and micrometer/nanometer HZSM-5 zeolites. *Appl. Catal., A* **2006**, *305* (2), 176−188.
(23) Cadenas, M.; Bringué, R.; Fité, C.; Ramírez, E.; Cunill, F. Liquid-phase oligomerization of 1-hexene catalyzed by macroporous ion-exchange resins. *Top. Catal.* **2011**, *54* (13−15), 998−1008.
(24) Bringué, R.; Cadenas, M.; Fité, C.; Iborra, M.; Cunill, F. Study of the oligomerization of 1-octene catalyzed by macroreticular ion-exchange resins. *Chem. Eng. J.* **2012**, *207-208*, 226−234.
(25) Finiels, A.; Fajula, F.; Hulea, V. Nickel-based solid catalysts for ethylene oligomerization − a review. *Catal. Sci. Technol.* **2014**, *4* (8), 2412−2426.
(26) de Klerk, A. Oligomerization of 1-hexene and 1-octene over solid acid catalysts. *Ind. Eng. Chem. Res.* **2005**, *44* (11), 3887−3893.
(27) Wight, A. P.; Davis, M. E. Design and preparation of organic−inorganic hybrid catalysts. *Chem. Rev.* **2002**, *102* (10), 3589−3614.
(28) del Pozo, C.; Corma, A.; Iglesias, M.; Sánchez, F. Immobilization of (NHC) NN-pincer complexes on mesoporous MCM-41 support. *Organometallics* **2010**, *29* (20), 4491−4498.
(29) Kermagoret, A.; Kerber, R. N.; Conley, M. P.; Callens, E.; Florian, P.; Massiot, D.; Delbecq, F.; Rozanska, X.; Copéret, C.; Sautet, P. Chlorodiethylaluminum supported on silica: A dinuclear aluminum surface species with bridging μ^2-Cl-ligand as a highly efficient co-catalyst for the Ni-catalyzed dimerization of ethane. *J. Catal.* **2014**, *313*, 46−54.
(30) Li, Z.; Ma, X.; Liu, J.; Feng, X.; Tian, G.; Zhu, A. Silica-supported aluminum chloride: A recyclable and reusable catalyst for one-pot three-component Mannich-type reactions. *J. Mol. Catal. A: Chem.* **2007**, *272* (1−2), 132−135.
(31) Zhao, X. S.; Lu, M. G. Q.; Song, C. Immobilization of aluminum chloride on MCM-41 as a new catalyst system for liquid-phase isopropylation of naphthalene. *J. Mol. Catal. A: Chem.* **2003**, *191* (1), 67−74.
(32) Wang, Z.; Gao, B. Preparation, structure, and catalytic activity of alumina chloride immobilized on cross-linked polyvinyl alcohol microspheres. *J. Mol. Catal. A: Chem.* **2010**, *330* (1−2), 35−40.
(33) Sun, H.; Shen, B.; Wu, D.; Guo, X.; Li, D. Supported Al-Ti bimetallic catalysts for 1-decene oligomerization: Activity, stability and deactivation mechanism. *J. Catal.* **2016**, *339*, 84−92.
(34) Zhu, H. *Preparation and Application of Catalyst Support*; Petroleum Industry Press: Beijing, 2002.
(35) Tsakoumis, N. E.; Johnsen, R. E.; van Beek, W.; Rønning, M.; Rytter, E.; Holmen, A. Capturing metal-support interactions in situ during the reduction of a Re promoted Co/γ-Al_2O_3 catalyst. *Chem. Commun.* **2016**, *52* (15), 3239−3242.
(36) Safari, J.; Khalili, S. D.; Banitaba, S. H. Three Component, One-Pot Synthesis of 2,4,5-Trisubstituted Imidazoles Catalyzed by $TiCl_4$-SiO_2 Under Conventional Heating Conditions or Microwave Irradiation. *Synth. Commun.* **2011**, *41* (16), 2359−2373.
(37) Peng, Y.; Dong, M.; Meng, X.; Zong, B.; Zhang, J. Light FCC Gasoline Olefin Oligomerization over a Magnetic $NiSO_4$/γ-Al_2O_3 Catalyst in a Magnetically Stabilized Bed. *AIChE J.* **2009**, *55* (3), 717−725.
(38) Zhang, Z.; Zhang, Q.; Jia, L.; Wang, W.; Gao, X.; Gu, Y.; Gao, X.; Han, Y.; Tan, Y. Regulation of SBA-15, g-Al_2O_3, ZSM-5 and MgO

DOI: 10.1021/acs.iecr.8b00791
Ind. Eng. Chem. Res. 2018, 57, 6664−6672

on Molybdenum oxide and Consequent Effect on DME Oxidation Reaction. *ChemistrySelect* **2016**, *1* (19), 6127−6135.
(39) Borujeni, K. P.; Tamami, B. Polystyrene and silica gel supported $AlCl_3$ as highly chemoselective heterogeneous Lewis acid catalysts for Friedel-Crafts sulfonylation of aromatic compounds. *Catal. Commun.* **2007**, *8* (8), 1191−1196.
(40) Kissin, Y. V. Multicenter nature of titanium-based Ziegler-Natta catalysts: Comparison of ethylene and propylene polymerization reactions. *J. Polym. Sci., Part A: Polym. Chem.* **2003**, *41* (12), 1745−1758.
(41) Chammingkwan, P.; Thang, V. Q.; Terano, M.; Taniike, T. $MgO/MgCl_2/TiCl_4$, Core−Shell Catalyst for Establishing Structure-Performance Relationship in Ziegler−Natta Olefin Polymerization. *Top. Catal.* **2014**, *57* (10−13), 911−917.
(42) Kashiwa, N.; Tsutsui, T. Highly active MgO-supported $TiCl_4$, catalyst for the ethylene polymerization. *Polym. Bull.* **1984**, *11* (4), 313−317.
(43) Lassaletta, G.; Caballero, A.; Wu, S.; González-Elipe, A. R.; Fernández, A. Photoelectron spectroscopy of metal oxide particles: size and support effects. *Vacuum* **1994**, *45* (10−11), 1085−1086.
(44) Leinen, D.; Lassaletta, G.; Fernández, A.; Caballero, A.; González-Elipe, A. R.; Martin, J. M.; Vacher, B. Ion beam induced chemical vapor deposition procedure for the preparation of oxide thin films. II. Preparation and characterization of $Al_xTi_yO_z$ thin films. *J. Vac. Sci. Technol., A* **1996**, *14* (5), 2842−2848.
(45) Zhou, C. H.; Li, G. L.; Zhuang, X. Y.; Wang, P. P.; Tong, D. S.; Yang, H. M.; Lin, C. X.; Li, L.; Zhang, H.; Ji, S. F.; Yu, W. H. Roles of texture and acidity of acid-activated sepiolite catalysts in gas-phase catalytic dehydration of glycerol to acrolein. *Mol. Catal.* **2017**, *434*, 219−231.
(46) Krishna, V.; Naresh, G.; Kumar, V. V.; Sarkari, R.; Padmasri, A. H.; Venugopal, A. Synthesis of 2,6-dimethylpyrazine by dehydrocyliza-tion of aqueous glycerol and 1,2-propanediamine over Cu-Cr-O catalyst: Rationalization of active sites by pyridine and formic acid adsorbed IR studies. *Appl. Catal., B* **2016**, *193*, 58−66.
(47) Li, W.; Fan, G.; Yang, L.; Li, F. Surface Lewis acid-promoted copper-based nanocatalysts for highly efficient and chemoselective hydrogenation of citral to unsaturated allylic alcohols. *Catal. Sci. Technol.* **2016**, *6* (7), 2337−2348.
(48) Xu, T.; Kob, N.; Drago, R. S.; Nicholas, J. B.; Haw, J. F. A Solid Acid Catalyst at the Threshold of Superacid Strength: NMR, Calorimetry, and Density Functional Theory Studies of Silica-Supported Aluminum Chloride. *J. Am. Chem. Soc.* **1997**, *119* (50), 12231−12239.
(49) Getty, E. E.; Drago, R. S. Preparation, characterization, and catalytic activity of a new solid acid catalyst system. *Inorg. Chem.* **1990**, *29* (6), 1186−1192.
(50) Choudhary, V. R.; Mantri, K. $AlCl_3$-grafted Si-MCM-41: influence of thermal treatment conditions on surface properties and incorporation of Al in the structure of MCM-41. *J. Catal.* **2002**, *205* (1), 221−225.
(51) Krzywicki, A.; Marczewski, M. Superacidity of modified γ-Al_2O_3. Structure of active site and catalytic activity. *J. Chem. Soc., Faraday Trans. 1* **1980**, *76*, 1311−1322.
(52) Lu, L.; Niu, H.; Dong, J. Propylene polymerization over $MgCl_2$-supported $TiCl_4$ catalysts bearing different amounts of a diether internal electron donor: extrapolation to the role of internal electron donor on active site. *J. Appl. Polym. Sci.* **2012**, *124* (2), 1265−1270.
(53) Haukka, S.; Lakomaa, E. L.; Root, A. An IR and NMR study of the chemisorption of titanium tetrachloride on silica. *J. Phys. Chem.* **1993**, *97* (19), 5085−5094.
(54) Cai, T.; He, M. New approaches to immobilization of aluminum chloride on γ-alumina and its regeneration after deactivation. *Catal. Lett.* **2003**, *86* (1−3), 17−23.
(55) Dubé, D.; Royer, S.; Béland, F.; Kaliaguine, S. Aluminum chloride grafted mesoporous molecular sieves as alkylation catalysts. *Microporous Mesoporous Mater.* **2005**, *79* (1−3), 137−144.
(56) Huang, Q.; Chen, L.; Ma, L.; Fu, Z.; Yang, W. Synthesis and Characterization of oligomer from 1-decene catalyzed by supported Ziegler-Natta catalyst. *Eur. Polym. J.* **2005**, *41* (12), 2909−2915.
(57) Huang, Q.; Chen, L.; Sheng, Y.; Ma, L.; Fu, Z.; Yang, W. Synthesis and Characterization of Oligomerization from 1-Decene Catalyzed by $AlCl_3/TiCl_4/SiO_2/Et_2AlCl$. *J. Appl. Polym. Sci.* **2006**, *101* (1), 584−590.

DOI: 10.1021/acs.iecr.8b00791
Ind. Eng. Chem. Res. 2018, 57, 6664−6672